EXPERIMENTAL CHARACTERIZATION OF NOZZLE FLOW EXPANSIONS OF SILOXANE MM FOR ORC TURBINES APPLICATIONS

Giorgia Cammi[1], Camilla Cecilia Conti[1,2], Andrea Spinelli[1*], Fabio Cozzi[1] and Alberto Guardone [2]

[1] Department of Energy
Politecnico di Milano
Via Lambruschini, 4, 20156 Milano, Italy

[2] Department of Aerospace Science and Technology,
Politecnico di Milano
Via La Masa 34, 20156 Milano, Italy

* andrea.spinelli@polimi.it (E-mail)

ABSTRACT

This paper reports extensive experimental results characterizing the supersonic expansion of organic vapor MM (hexamethyldisiloxane, $C_6H_{18}OSi_2$) in conditions representative of actual Organic Rankine Cycle (ORC) turbines operations, in the close proximity of the liquid-vapor saturation curve. Experiments were conducted on the Test Rig for Organic VApors (TROVA), at the Laboratory of Compressible fluid-dynamics for Renewable Energy Applications (CREA Lab) of Politecnico di Milano. Two different planar nozzles were tested, featuring an exit Mach number of 1.5 and 1.6. Nozzle flow expansions were characterized by measuring total pressure, total temperature, static pressures along the nozzle axis and by performing schlieren visualizations. It was verified that the expansion is influenced by total inlet conditions due to the non-ideal nature of the flow. Data were analysed to assess the influence of the total compressibility factor and the effect of total temperature. Since the nozzle with exit Mach number equal to 1.5 was also tested in a previous experimental campaign (Spinelli et al. (2018)) with siloxane fluid MDM (octamethyltrisiloxane, $C_8H_{24}O_2Si_3$), a comparison between the behaviour of the two fluids was also carried out. The present experimental investigation provides significant validation data for the improvement of state-of-the-art thermodynamic models and of design tools for siloxane fluids in general and for siloxane MM in particular.

1. INTRODUCTION

Organic Rankine Cycle (ORC) power systems are a convenient option for power production in the 1 to 100 MW range when low/medium source temperatures are involved, thanks to their relatively high efficiency, low cost and plant simplicity with respect to traditional steam Rankine cycles. Such temperatures and power ranges are often found in the case of renewable energy sources, such as geothermal reservoirs, biomass combustion and waste heat recovery from several industrial processes (power plants, cement and glass factories) (Colonna et al. (2015); Macchi and Astolfi (2017); Tartiere and Astolfi (2017)).
ORCs involve flows of heavy and complex organic compounds in thermodynamic regions close to the liquid-vapor saturation curve and to the critical point, where intermolecular forces are not negligible. As a result, ORC turbine flows differ from standard turbomachinery ones because they are highly supersonic and show significant non-ideal gas effects, such as flow field dependence on stagnation conditions (Spinelli et al. (2018, 2019); Colonna et al. (2008)). Given this, the design of such machines is particularly critical, also considering that turbine efficiency impacts the economic competitiveness of the ORC technology. Current computational tools are based on advanced CFD codes (Vitale et al. (2015); Pini et al. (2015); Vitale et al. (2018); Persico et al. (2015)) embedding state-of-the-art thermodynamic

models (Span and Wagner (2003); Thol et al. (2017)), but experimental data are only recently becoming available in literature for comparison and verification (Spinelli et al. (2018, 2019); Dura Galiana et al. (2016)). This is mainly due to the peculiar features of organic fluid flows, as the high temperature, the vicinity to the saturation curve and to the thermal stability limits, challenging the success of ad-hoc experimental campaigns. Thus, recently, several experimental facilities have been constructed such as the FAST (Mathijssen et al. (2015)) and ORCHID (Head et al. (2016)) facilities at TU Delft, the CLOWT (Reinker et al. (2017)) at Muenster University of Applied Sciences and the Test Rig for Organic VApors (TROVA) Spinelli et al. (2013) at the Laboratory of Compressible fluid-dynamics for Renewable Energy Applications (CREA Lab) of Politecnico di Milano.

In particular, the TROVA is a blow-down wind tunnel specifically designed and constructed to reproduce supersonic flows of organic vapors in conditions representative of ORC turbine expansions, in order to contribute to the available bibliography on experimental data in the ORC field. The TROVA test section can be equipped with planar nozzles, designed for different fluids and/or operating conditions, and it can also accommodate linear blade cascades. In the present experimental campaign, two different nozzles were tested with siloxane fluid MM (hexamethyldisiloxane, $C_6H_{18}OSi_2$), yielding a design exit Mach number of 1.5 and 1.6 (typical values for ORC turbine vanes, especially for initial stages). Nozzle expansions were characterized by total temperature and total pressure measures, by static pressure measurement along the center line and by the Schlieren technique to visualize the two-dimensional density gradient field along the axis direction. A wide range of inlet conditions was explored in order to systematically span the thermodynamic region included between the saturation curve and the critical temperature. Conditions varied from highly non-ideal to almost ideal gas conditions, with a compressibility factor evaluated at total conditions (*total compressibility*, Z_T) ranging between 0.57 and 0.98.

Results from the present experimental campaign allowed to verify that nozzle expansion is influenced by total inlet conditions because of the non-ideal nature of the flow. It was investigated whether total compressibility alone is sufficient to assess the level of non-ideality of a nozzle flow and thus, to characterize the expansion and predict pressure ratio profiles. Also, the effect of total temperature was isolated and analyzed in depth. Moreover, the nozzle with exit Mach number equal to 1.5 was also tested in a previous experimental campaign (Spinelli et al. (2018)) with siloxane fluid MDM (octamethyltrisiloxane, $C_8H_{24}O_2Si_3$). It was thus possible to carry out a comparison of two different organic vapors flowing in the same nozzle and sharing the same total reduced conditions.

The paper is structured as follows. Section 2 describes the facility, the implemented measurement techniques and the selected test conditions. Results showing non-ideal gas effects are presented in Section 3, while the influence of the total compressibility factor is discussed in Section 4. The effect of total temperature on nozzle flow is analyzed in Section 5 and a comparison between MM and MDM nozzle expansions is reported in Section 6. Section 7 finally draws the conclusions of this work.

2. EXPERIMENTAL SET-UP

2.1 The Test-Rig for Organic Vapors (TROVA)

The Test-Rig for Organic Vapors (TROVA) is a blow-down wind tunnel specifically designed to reproduce flows of non-ideal vapors in conditions representative of ORC turbines expansions. The working fluid is isochorically heated in a High Pressure Vessel (HPV) until the desired temperature and pressure conditions. The vapor is discharged at the opening of the Main Control Valve (MCV) from the HPV to a Low Pressure Vessel (LPV) by passing through a settling chamber (plenum) and then a test section, in which it is expanded from subsonic to supersonic velocity through a converging-diverging nozzle. The vapor is condensed in the LPV and pumped back to the HPV by means of a membrane pump. More details on the design and operation of the TROVA can be found in Spinelli et al. (2013).

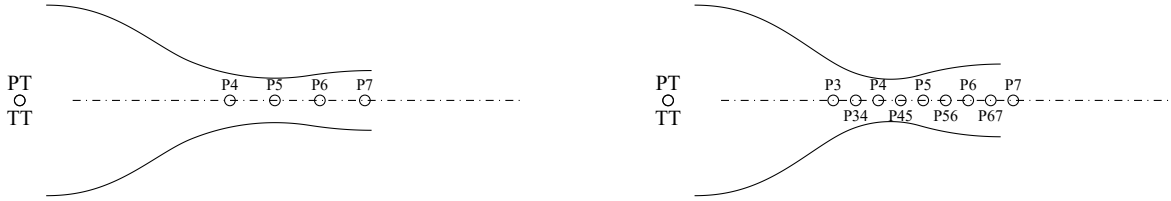

(a) Nozzle $M1.5$: sketch of the nozzle profile with measurement points position.

(b) Nozzle M1.6: sketch of the nozzle profile with measurement points position.

Figure 1: Nozzles tested.

2.2 Test Section

The TROVA test section is planar and it can accommodate straight-axis nozzles with a rectangular cross-section, designed for the considered fluid and operating conditions according to the procedure described in Guardone et al. (2013). The straight-axis geometry allows to characterize the flow field at the nozzle core during regimes where shock waves inside the nozzle are absent by using the isentropic flow hypothesis, thus avoiding the need for calibrated pressure probes, which are currently not available for organic vapors flows. Two nozzles were tested. One nozzle, called $M1.5$ (Fig. 1a), was designed during previous experimental campaigns (see Spinelli et al. (2018, 2019)) for siloxane fluid MDM (octamethyltrisiloxane, $C_8H_{24}O_2Si_3$) to deliver a uniform exit flow with Mach number $M = 1.5$. It is characterized by a nozzle semi-height $H = 8.4\ mm$. This nozzle was tested with both MDM and MM, and comparison between the two fluids behaviour is reported in Section 6. The second nozzle is labeled $M1.6$ (Fig. 1b) and was designed for siloxane fluid MM with $H = 8\ mm$ to produce a uniform exit flow with $M = 1.6$.

2.3 Measurements Setup and Instrumentation

16 pressure taps of 0.3 mm in diameter are machined onto the rear steel plate along the nozzle axis. Each tap is connected to a pressure transducer through a ≈ 50 mm long line, providing a measure of the wall static pressure. Not all taps are simultaneously active during a single test. Nozzle total pressure and temperature (P_T and T_T respectively) are measured in the plenum upstream of the test section, where flow velocity is low enough (about 1 m/s) to make the kinetic energy negligible. Thus, P_T is measured with a wall pressure transducer and T_T with the use of two thermocouples, one of K-type (hot junction 0.15 mm) and one of J-type (hot junction 0.25 mm), with hot junctions placed at the chamber axis at 200 mm distance from one another. Pressure transducers are of piezo-resistive type. Due to their temperature sensitivity, they were calibrated both in pressure and temperature from 1 bar to full scale (3.5 ≤FS≤ 40 bar) and from 25°C to 300°C. Thermocouples were calibrated in the same temperature range (25-300 °C). The expanded uncertainty is of the order of 0.07 % of the full scale for pressure sensors and of about 1 °C for thermocouples. Data sampling frequency for temperature and pressure measurements is 1 kHz. Further details on instrumentation can be found in Spinelli et al. (2018).

2.4 Test Description and Conditions

Each test starts as the MCV is opened and flow discharge through the nozzle occurs. Test time is about 140 s, excluding the valve opening transient (about 2 s). Tests end as the nozzle reaches over-expanded conditions with shocks waves entering in the nozzle. Since no control on total pressure is operated, P_T and T_T decrease in time as the HPV empties and a wide range of thermodynamic states are explored during a single test run, from initial strong non-ideal conditions to the ideal gas state. Nozzle relaxation time is more than two orders of magnitude lower than the emptying time of the HPV (Spinelli et al. (2013)), so that the nozzle flow can be assumed in a steady state at each sampled instant. To illustrate this, Figure 2a reports different total conditions, all belonging to the same test. Going from condition *a* to condition *h*, as the test proceeds, total pressure and temperature decrease indeed. Consequently the total compressibility factor, defined in equation 1 where R_{fluid} is the gas constant and $\rho_T = \rho(T_T, P_T)$ is

Test ID	Nozzle	Most non-ideal condition			Least non-ideal condition		
		$P_T\,[bar]$	$T_T\,[°C]$	Z_T	$P_T\,[bar]$	$T_T\,[°C]$	Z_T
14MM	*M1.5*	12.292	223.3	0.64	2.314	221.7	0.95
19MM	*M1.5*	7.386	193.8	0.76	1.425	195.9	0.96
21MM	*M1.6*	10.576	222.1	0.71	0.840	215.5	0.98
30MM	*M1.6*	7.796	206.8	0.77	0.570	202.9	0.99
31MM	*M1.6*	6.266	185.3	0.78	0.654	193.5	0.98
33MM	*M1.6*	12.290	234.5	0.69	1.605	221.7	0.96
40MM	*M1.6*	18.971	259.4	0.57	2.632	234.5	0.95

Table 1: Tests selected for analysis in the present paper

the stagnation density, increases towards unity during the test.

$$Z_T = \frac{P_T}{T_T R_{fluid} \rho(T_T, P_T)} \tag{1}$$

The equation of state used within this paper to obtain thermodynamic quantities starting from measured quantities is the one presented in Thol et al. (2017). The compressibility factor Z identifies how far the volumetric behaviour of a flow is from that of an ideal gas. Thus, it can be used to quantify the level of flow non-ideality. Each total condition reported in Figure 2a refers to the corresponding isentropic expansions plotted in Figure 2b.

Several tests were performed and flows characterized by the same total conditions were reported in different test. Comparison of this data proved consistency and repeatability of the performed measurements. Among all tests carried out during the experimental campaign, 7 were selected for analysis in the present paper: Tests *14MM*, *19MM* performed with nozzle *M1.5* and Tests *21MM*, *30MM*, *31MM*, *33MM*, *40MM* performed with nozzle *M1.6*. They are summarized in table 1 which also reports the most and the least non-ideal total conditions reached in each of these tests, corresponding to the first and last total conditions measured.

3. EVIDENCE OF NON-IDEAL GAS EFFECTS

Test 40MM achieved the most non-ideal total conditions of the whole experimental campaign. Nozzle expansions characterized by total compressibility factors, ranging from $Z_T^{min} = 0.57$ to $Z_T^{max} = 0.95$ were extracted from this test. Figure 2a reports the total conditions at which data were analysed on a $P - T$ diagram with Z contours, with points labeled from 'a' to 'h' at increasing values of Z_T, so at increasing levels of ideality. Figure 2b shows the corresponding isentropic expansions on a $T - s$ diagram.

Pressure ratio measured along the nozzle axis during these expansions can be used to prove the influence of non-ideal fluid effects. Indeed, following *quasi-1D* theory, if the ideal gas equation of state is applicable, pressure ratios along the nozzle axis are independent of total conditions. Thus, the pressure ratio change with total conditions can be ascribed to the so called non-ideal compressible fluid effects Colonna et al. (2008).

Figure 2c shows pressure ratio trends along the nozzle axis during test 40MM. Pressure ratios decrease going from the most non-ideal condition *40MMa*, characterized by $Z_T^{min} = 0.57$, to the most ideal one *40MMh*, featuring a $Z_T^{max} = 0.95$ much closer to the ideal gas limit of 1. A zoom (Figure 2d) on the first pressure tap after the geometrical throat (located at $x/H = 9.26$) clearly shows that the P/P_T change is larger than experimental uncertainty, since error bars do not overlap, thus proving that the trend is indeed

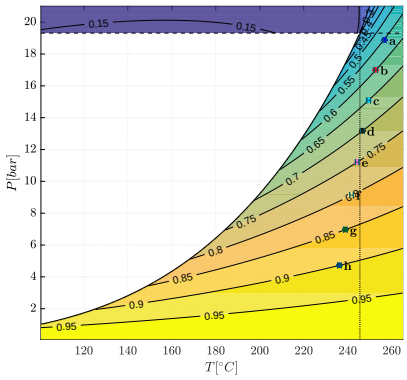

(a) Total conditions plotted on a $P-T$ diagram for MM together with a Z contour, the saturation curve (black line), critical pressure (dashed black line) and critical temperature (dotted black line).

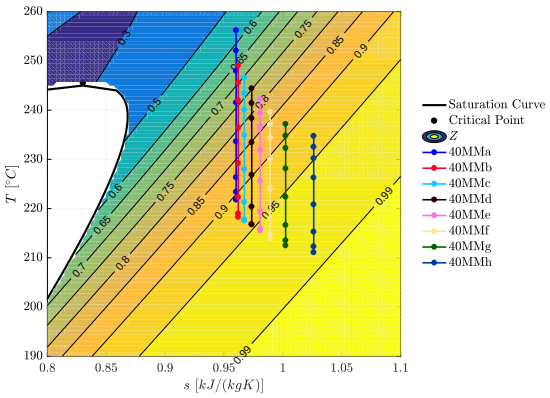

(b) Isentropic nozzle expansions plotted on a T–s diagram together with the saturation curve (black line) . The dots along each expansion correspond to temperatures computed using the static pressure measured along the axis.

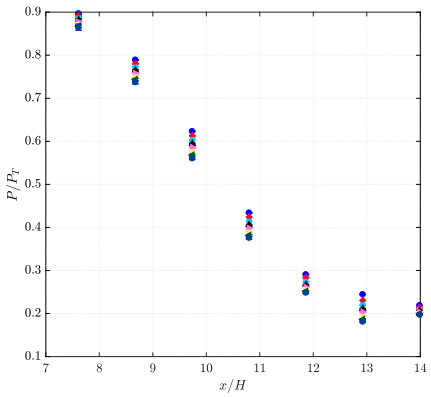

(c) P/P_T trends along the nozzle axis extracted from test *40MM*.

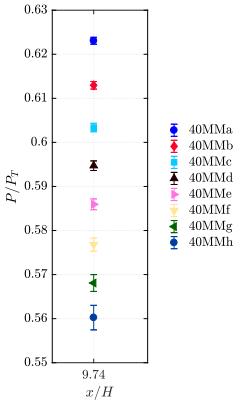

(d) Zoom at x/H = 9.74 (pressure tap downstream the geometrical throat).

Figure 2: Analysis of different flows extracted from test *40MM*.

to be attributed to non-ideal effects. The difference between the pressure ratio measured at the most non-ideal and at the most ideal total conditions grows going from nozzle inlet up to x/H = 12.93, where the pressure ratio at Z_T^{min} is 1.35 times the one at Z_T^{max}. Analogous results were found also in the experimental campaign conducted on the TROVA using MDM as working fluid, as reported in Spinelli et al. (2018).

4. INFLUENCE OF TOTAL COMPRESSIBILITY FACTOR Z_T ON MM NOZZLE EXPANSIONS

Results presented in Section 3 prove the dependence of pressure ratio profiles on the total conditions at which the nozzle is operated, univocally characterized by total pressure P_T and total temperature T_T. The total compressibility factor can be used as a non-dimensional parameter to characterize the volumetric behaviour of a non-ideal gas at a specific thermodynamic point. Conditions for different tests were chosen so as to acquire experimental data of expansions at different total conditions P_T and T_T but same total compressibility factor Z_T, in order to investigate whether parameter Z_T alone is sufficient to assess the level of non-ideality of a nozzle flow and thus, to characterize the expansion and predict pressure ratios. Figure 3a reports the total conditions of selected nozzle flows at several values of Z_T and from different tests. The comparisons between pressure ratio profiles of different tests at different total conditions and

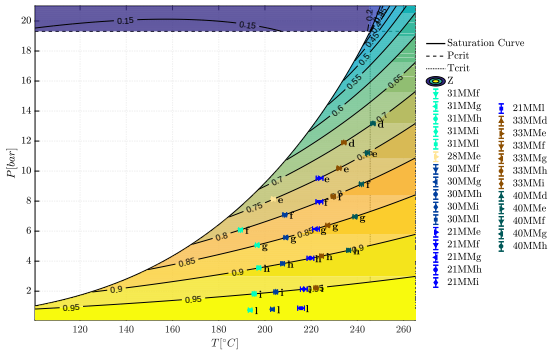

(a) Total conditions characterizing the nozzle flows analyzed .

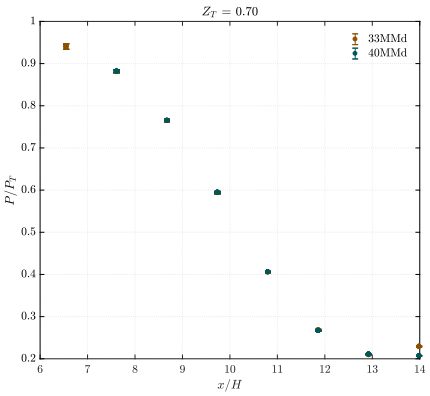

(b) Pressure ratio profiles along the nozzle axis for all different total conditions sharing $Z_T = 0.70$.

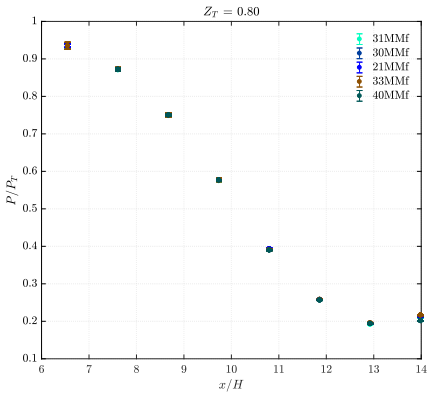

(c) Pressure ratio profiles along the nozzle axis for all different total conditions sharing $Z_T = 0.80$.

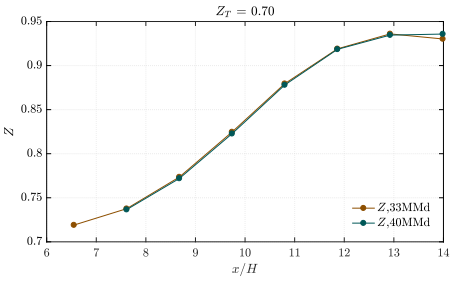

(d) Profiles of Z along the nozzle axis for all different total conditions sharing $Z_T = 0.70$.

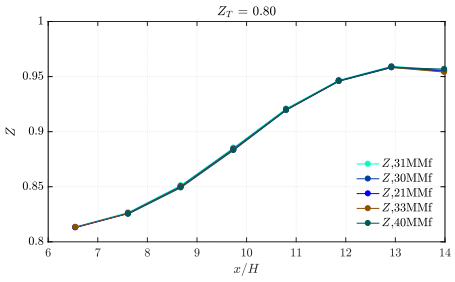

(e) Profiles of Z along the nozzle axis for all different total conditions sharing $Z_T = 0.80$.

Figure 3: Assessment of the influence of the total compressibility factor Z_T on pressure ratio P/P_T. Comparison is made at constant Z_T and varying (P_T, T_T)

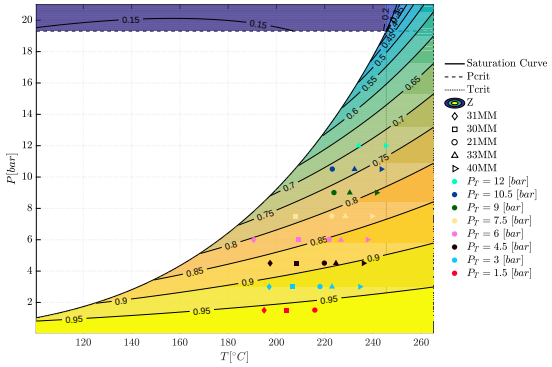

(a) Total conditions characterizing the nozzle flows analyzed to assess the influence of the total temperature T_T on pressure ratios.

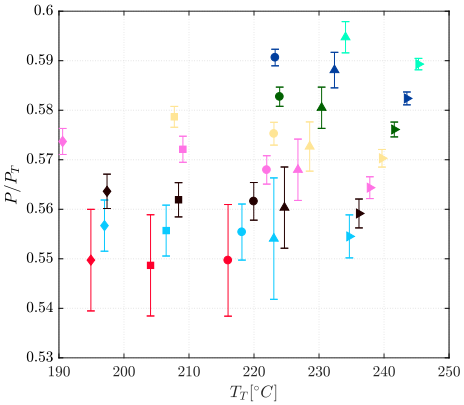

(b) Data at pressure tap located at x/H = 9.74. Different colors represent different total pressures while different markers belong to different tests as reported in the legend of Figure 4a.

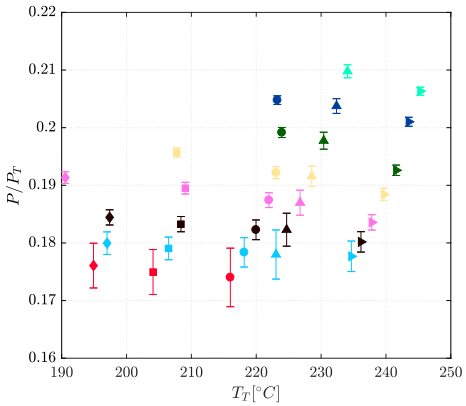

(c) Data at pressure tap located at x/H = 12.93. Different colors represent different total pressures while different markers belong to different tests as reported in the legend of Figure 4a.

Figure 4: Pressure ratios plotted against total temperatures. Each data series is taken at the same total pressure. The two figures refer to two different axial locations on the nozzle axis.

same Z_T are reported in Figure 3b for Z_T = 0.70 (corresponding to label 'd' for all tests) and in Figure 3c for Z_T = 0.80 (corresponding to label 'f' for all tests). The number of pressure ratio profiles at Z_T = 0.70 is lower than for Z_T = 0.80 because lower Z_T values are confined to a smaller thermodynamic region closer to the critical point (see Fig. 3a). It can be noticed that pressure ratio profiles are almost superimposed except from the last available axial position at x/H = 13.99. Figures 3d and 3e report the profile of the compressibility factor Z computed using the static pressures measured along the nozzle axis. In principle starting from the same value of Z_T does not necessarily results in obtaining the same Z profiles. However, for the conditions analyzed the resulting Z profile are superimposed except in the last axial location x/H = 13.99, thus explaining the pressure profiles deviation.

By looking at the whole data set spacing from Z_T = 0.70 to Z_T = 0.98 (plots not reported for brevity) it is confirmed that, within the thermodynamic region explored, pressure ratio profiles of nozzle flows characterized by same Z_T are superimposed with the only exception of the last axial coordinate analysed. In this region near the nozzle exit, pressure ratio can no longer be considered dependent on Z_T only, but also T_T and P_T play a role. However their influence reduces going towards expansions characterized by larger Z_T and it vanishes at Z_T = 0.98.

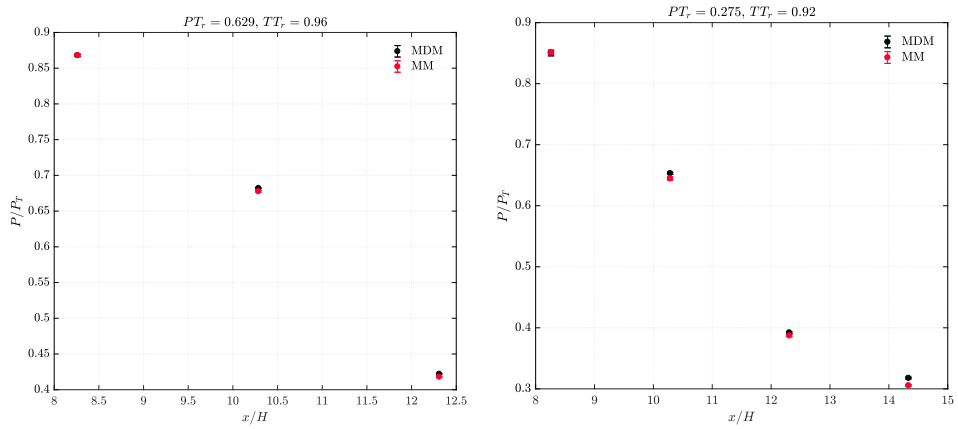

(a) Profiles of pressure ratio.

(b) Profiles of pressure ratio.

Figure 5: Comparison between nozzle flows of non-ideal compressible vapors MDM and MM.

5. INFLUENCE OF TOTAL TEMPERATURE ON MM NOZZLE EXPANSIONS

In ORC turbines, the total inlet temperature can vary by effect of different levels of super-heating. For this reason, it is of interest for off-design turbine operation to estimate how such variation affects the flow expansion. The influence of total temperature can be isolated by comparing pressure ratios of tests in conditions having same total pressure, but different T_T. Figure 4a reports all total conditions of nozzle expansions analyzed to assess the influence of T_T.

In Figures 4b, 4c pressure ratios measured at different total temperatures but same total pressure are shown at two particular positions along the nozzle axis. Figure 4b refer to axial location x/H = 9.74 located right after the geometrical throat on the nozzle while figure 4c refers to axial location x/H = 12.93 placed in the supersonic portion of the nozzle. Each color identifies the P_T at which the different measurements were taken. It can be seen that the light blue and the red dots referring to P_T = 3 $[bar]$ and P_T = 1.5 $[bar]$ show a greater uncertainty. This is related to the batch nature of the TROVA facility; indeed transducers must withstand higher pressures which decreases during the experiment. The uncertainty on the pressure ratio P/P_T is proportional to the relative uncertainty of P and P_T, which both increse as the test proceeds since the absolute uncertainty of each sensor is related to the full scale and almost independent of the measured value of pressure, which decreases as the test proceeds.

A clear trend can be noticed in figures 4b, 4c: the pressure ratio increases as the total temperature decreases. This is consistent with the fact that a lower T_T at constant P_T leads to lower total compressibility factors, thus higher non-ideal effects. Moreover the influence of a change in the total temperature is stronger in thermodynamic regions closer to the critical point due to higher Z variation for the same change in temperature. Indeed, as the total pressure decreases, pressure ratio trends with total temperature flatten and tend to remain constant (blue and red dots in Figures 4b, 4b), consistently with the approaching of ideal conditions.

6. COMPARISON BETWEEN MM AND MDM NOZZLE EXPANSIONS

Nozzle *M1.5* was also used in a previous experimental campaign conducted with fluid MDM and presented in Spinelli et al. (2018, 2019). Test conditions with this same nozzle and fluid MM were chosen in order to have the same total initial reduced conditions ($T_{Tr} = T_T/T_{critical}, P_{Tr} = P_T/P_{critical}$) as for fluid MDM to allow a comparison between the expansions of the two fluids. All total conditions considered for the comparison are listed in Table 2.

The Van der Waals equation of state is the simplest one capable of modeling non-ideal compressible effects. Its simplicity makes it a powerful tool for making qualitative considerations even though its quantitative accuracy is lower than other more complex equation of states. Following the Van der Waals

		MM			MDM		
T_r	P_r	T_T [°C]	P_T [bar]	Z_T	T_T [°C]	P_T [bar]	Z_T
0.96	0.63	222.4	12.162	0.656	268.97	9.044	0.652
0.97	0.522	229.1	10.071	0.746	275.57	7.494	0.756
0.97	0.434	228.6	8.380	0.797	275.31	6.240	0.806
0.967	0.335	227.1	6.475	0.848	273.39	4.814	0.855
0.96	0.228	224.7	4.397	0.899	270.61	3.272	0.904
0.92	0.275	202.0	5.314	0.849	246.3	3.960	0.854
0.91	0.187	199.7	3.618	0.900	242.8	2.691	0.892

Table 2: Analysed conditions for comparison purposes between MM and MDM expansions.

model, two different fluids characterized by the same reduced conditions also share the same compressibility factor. If Z_T is computed with a more accurate, state-of-the-art equation of state (Thol et al. (2017)), values of the total compressiblity factor for conditions selected here for comparison differ by less than 1.5% between MM and MDM, as reported in table 2. This is an indication that the two fluids show a very similar volumetric behaviour if compared at same reduced total conditions. Indeed, pressure ratio profiles along the nozzle axis obtained for the analysed reduced conditions are almost superimposed, as shown in Figures 5a and 5b for two different total reduced condition. The maximum difference is located in the last pressure tap x/H = 14.33, whose measurements are available only in figure 5b.
It can be concluded, by analysing quantitatively the differences, both in term of pressure ratios and of Mach number (not reported here) on the axis, between the two fluids,that, in the thermodynamic region covered, the pressure ratio differences are lower than 5% for the axial coordinate x/H = 14.33 and lower than 1.5% for all others. Moreover the lower value of P/P_T is always achieved with fluid MM, as expected since it is less complex than fluid MDM.

7. CONCLUSIONS

Results of an extensive experimental campaign carried out with siloxane MM (hexamethyldisiloxane, $C_6H_{18}OSi_2$) were presented. The campaign analyzed the expansion inside two different nozzles: *M1.6* and *M1.5*. Results of nozzle *M1.6* were used first to highlight the experimental evidence of non-ideal gas effects making the pressure ratio profile dependent on the total conditions.
Comparisons between pressure ratio profiles of different tests at different total conditions and same Z_T were carried out in order to assess whether parameter Z_T alone is sufficient to characterize the expansion and predict pressure ratios. It was concluded that, in the thermodynamic region explored, pressure ratio can be considered as a function only of Z_T with an error lower than 5%.
The influence of total temperature on the flow was analyzed by comparing pressure ratios of tests in conditions having same total pressure, but different T_T. A clear trend was found: the pressure ratio increases as the total temperature decreases, consistently with consequent change in Z_T.
The results from nozzle *M1.5* were used to perform a comparison between MM and MDM nozzle flows at the same total reduced conditions. Data of MDM nozzle expansions were collected in a previous experimental campaign (Spinelli et al. (2018)). It was concluded that, in the thermodynamic region explored pressure ratio profile of MM and MDM flows differ less than 1.5% for all axial coordinate up to x/H = 12.3 and less than 5% in x/H = 14.33.
The present experimental investigation provides significant validation data for the improvement of state-of-the-art thermodynamic models and of design tools for siloxane fluids in general and for siloxane MM in particular.

REFERENCES

Colonna, P., Casati, E., Trapp, C., Mathijssen, T., Larjola, J., Turunen-Saaresti, T., and Uusitalo, A. (2015). Organic rankine cycle power systems: From the concept to current technology, application, and an outlook to the future. Journal of Engineering for Gas Turbine and Power, 137:100801–100801–19.

Colonna, P., Harinck, J., Rebay, S., and Guardone, A. (2008). Real-gas effects in organic rankine cycle turbine nozzles. Journal of Propulsion and Power, 24:282–294.

Dura Galiana, F. J., Wheeler, A. P. S., and Ong, J. (2016). A study of trailing-edge losses in organic rankine cycle turbines. Journal of Turbomachinery, 138.

Guardone, A., Spinelli, A., and Dossena, V. (2013). Influence of molecular complexity on nozzle design for an organic vapor wind tunnel. Journal of Engineering for Gas Turbines and Power, 135.

Head, A. J., Servi, C. D., Casati, E., Pini, M., and Colonna, P. (2016). Preliminary design of the ORCHID: a facility for studying non-ideal compressible fluid dynamics and testing ORC expanders. Proceedings of ASME Turbo Expo.

Macchi, E. and Astolfi, M. (2017). Organic Rankine Cycle (ORC) Power Systems. Technologies and applications. Woodhead Publishing Series in Energy, New York.

Mathijssen, T., Gallo, M., Casati, E., Nannan, N. R., Zamfirescu, C., Guardone, A., and Colonna, P. (2015). The flexible asymmetric shock tube (FAST): a ludwieg tube facility for wave propagation measurements in high-temperature vapours of organic fluids. Experiments in Fluids, 56(10):195.

Persico, G., Pini, M., Dossena, V., and Gaetani, P. (2015). Aerodynamics of centrifugal turbine cascades. ASME J. Eng. Gas Turb. Power, 137(112602):1–11.

Pini, M., Persico, G., Pasquale, D., and Rebay, S. (2015). Adjoint method for shape optimization in real-gas flow applications. Journal of Engineering for Gas Turbines and Power, 137(3).

Reinker, F., Kenig, E. Y., Passmann, M., and aus der Wiesche, S. (2017). Closed loop organic wind tunnel (CLOWT): Design, components and control system. Energy Procedia, 129:200 – 207. 4th International Seminar on ORC Power SystemsSeptember 13-15th 2017.

Span, R. and Wagner, W. (2003). Equations of state for technical applications. II. Results for nonpolar fluids. International Journal of Thermophysics, 24(1):41–109.

Spinelli, A., Cammi, G., Conti, C. C., Gallarini, S., Zocca, M., Cozzi, F., Gaetani, P., Dossena, V., and Guardone, A. (2019). Experimental observation and thermodynamic modeling of non-ideal expanding flows of siloxane mdm vapor for orc applications. Energy, 168:285 – 294.

Spinelli, A., Cammi, G., Gallarini, S., Zocca, M., Cozzi, F., Gaetani, P., Dossena, V., and Guardone, A. (2018). Experimental evidence of non-ideal compressible effects in expanding flow of a high molecular complexity vapor. Experiments in Fluids, 59(8):126.

Spinelli, A., Pini, M., Dossena, V., Gaetani, P., and Casella, F. (2013). Design, simulation and construction of a test rig for organic vapors. ASME Journal of Engineering for Gas Turbine and Power, 135:042304–042304–10.

Tartiere, T. and Astolfi, M. (2017). A world overview of the organic rankine cycle market. Energy Procedia, 129:2 – 9. 4th International Seminar on ORC Power SystemsSeptember 13-15th 2017PO-LITECNICO DI MILANOBOVISA CAMPUSMILANO, ITALY.

Thol, M., Dubberke, F., Baumhögger, E., Vrabec, J., and Span, R. (2017). Speed of sound measurements and fundamental equations of state for octamethyltrisiloxane and decamethyltetrasiloxane. Journal of Chemical and Engineering Data, 62(9):2633–2648.

Vitale, S., Albring, T. A., Pini, M., Gauger, N. R., and Colonna, P. (2018). Fully turbulent discrete adjoint solver for non-ideal compressible flow applications. Journal of the Global Power and Propulsion Society, 1:252 – 270.

Vitale, S., Gori, G., Pini, M., Guardone, A., Economon, T. D., Palacios, F., Alonso, J. J., and Colonna, P. (2015). Extension of the SU2 open source CFD code to the simulation of turbulent flows of fuids modelled with complex thermophysical laws. In 22nd AIAA Computational Fluid Dynamics Conference, number AIAA Paper 2760.

ACKNOWLEDGEMENT

The research is funded by the European Research Council under ERC Consolidator Grant 2013, project NSHOCK 617603. The initial TROVA layout was funded by Turboden S.r.l..